RSC Advances

ROYAL SOCIETY OF CHEMISTRY

www.rsc.org/advances

RSC Advances

ARTICLE

Highly Efficient Performance of Activated Carbon Impregnated with Ag, ZnO and Ag/ZnO nanoparticles as Antimicrobial Materials

Received 00th January 20xx,
Accepted 00th January 20xx

DOI: 10.1039/x0xx00000x

www.rsc.org/

Prashantha Kumar T.K.M[a], Triveni R. Mandlimath[a], P. Sangeetha[a], P.Sakthivel[a], S.K. Revathi[a] S.K. Ashok Kumar[a*] and Suban K Sahoo[b]

A simple and efficient route for the synthesis of Ag, ZnO and Ag/ZnO nanostructures impregnated on highly porous activated carbon (AC) was developed. The antibacterial activities of AC, Ag-AC, ZnO-AC and Ag/ZnO-AC nanohybrids were evaluated against Gram negative and Gram positive bacteria's by the disc diffusion method. Among the four nanostructures, we found that Ag/ZnO-AC exhibited highest zone of inhibition, killing kinetics and post agent effect compared to the other nanohybrid materials. The minimum inhibitory concentration (MIC) and minimum bactericidal concentration (MBC) of Ag/ZnO-AC nanohybrid against standard reference cultures were found to be 0.20 mg/ml with *E. coli* and 0.30 mg/ml with *S.aureus* while MBC was found to be 0.35 mg/ml with *E. coli* and 0.6 mg/ml with *S.aureus.* The killing kinetics ($3\log_{10}$ decrease in 5 h) and post agent effect (2.45 h) were conducted only with *E. coli*. Ag/ZnO-AC nanohybrid material showed highest antimicrobial activity on selected microorganisms and the order of antibacterial activity was AC< ZnO-AC<Ag-AC<Ag/ZnO-AC.

1. Introduction

Water is the most abundant raw material on the Earth's surface. Since both the groundwater and surface water sources are equally susceptible to microbiological contamination from bacteria, protozoan and viruses, like any other raw material, water must be treated before consumption due to its universal solvency. World Health Organization (WHO) investigation has showed that 80% of the disease is due to contaminated drinking water. Further, WHO has recommended any water intended for drinking should contain fecal and total coli form counts of 0 in any 100 ml sample.[1] Organisms such as *Escherichia coli, Shigella spp., Salmonella spp., Vibrio spp.,* and *Cryptosporidium* are known to be transmitted by water and cause ill health in communities.[2] Even though advances in disinfection technology, already known and undiscovered pathogens moving into new areas continue to pose a great threat to human health, globally. Yet developed nations with more advanced water disinfection infrastructure continue to report disease outbreaks from waterborne infections.[3-6] Therefore, next generation disinfection technologies not only have to eliminate the emerging pathogens, but also remain cost-effective for large-scale adoption. Hence, inorganic antimicrobial materials can achieve appropriate disinfection without forming harmful by-products' and are more stable than organic antimicrobial agents.[7,8] As a consequence, the interest in inorganic antimicrobial materials such as metals and metal oxides has been growing in recent years.[9,10]

Metallic nanoparticles such as gold, silver, zinc, copper, titanium and palladium are among the most promising nanomaterials with bactericidal properties[11-16] owing to their charge capacity, high surface-to-volume ratios, crystallographic structure and adaptability to various substrates for increased contact efficiency.[17] Moreover, new combinational materials consisting of these nanometallic particles have been deployed among a number of substrates for their use in water disinfection.[18] Such materials as Ag deposited on titanium oxide, Ag-coated iron oxide and Ag loaded on zinc oxide had displayed faster kinetics and greater efficiency in eliminating bacteria.[19-21] The significance of the synergistic effect is not clear but researchers do report marked improvement in bactericidal effectiveness among these systems. Moreover, physically mixing the two metals does not increase the rate of reaction but if metal a doped on the surface of another metal then it forms galvanic couple that

[a] Materials Chemistry Division, School of Advanced Science, VIT University, Vellore-632014, India. Phone and Fax: +914162202352; +91 4162243092
E-mail: ashokkumar.sk@vit.ac.in
[b] Department of Applied Chemistry, SV National Institute Technology, Surat, Gujarat, India.

Electronic Supplementary Information (ESI) available: [details of any supplementary information available should be included here]. See DOI: 10.1039/x0xx00000x

increases the rate increase of the active metal and hence rate of reaction increases.[22,23]

One of the most important issues in antibacterial activity of Ag nanoparticles is release of Ag^+ ions from Ag nanoparticles, which is due to its oxidation in presence of water. Ag^+ ions release can be controlled to a certain extent by using an appropriate Ag particle size, that is, particles of 6 nm diameter have higher release (51%) in comparison to 25 nm diameter particles (5.8% release).[24] A second important issue is aggregation of Ag nanoparticles in the dispersion due to attractive inter particle and surface forces. In order to prevent aggregation and thereby maintain effective antibacterial activity, surfactants and polymers have been widely investigated. However, actual implementations are limited due to the high cost and biocompatibility issues of these additives.[25,26] Other inorganic materials such as TiO_2, ZnO, and Cu have also been investigated to understand their antibacterial properties.[27-29]

Recent reports in the literature comprise embedding of Ag and ZnO nanoparticles on various porous carbon materials including carbon nanotube, carbon aerogel, and activated carbon (AC) for inactivation of microbes as well as controlled release of Ag.[30,31] In these reports, Ag was found to be present on both the external surface of various porous carbons and also inside the pores in these various carbon-forms. However, surface engineering of carbon for selective embedding of Ag nanoparticles on the external surface as well as inside the porous of AC are required for efficient use of expensive, metallic Ag. This is due to bacteria (like *E. coli*) are of dimension of 1 µm or more, which would not be able to access Ag nanoparticles, whenever the latter are inside AC pores of size less than 1 µm. Also, when it is inside AC pores, they can be released slowly and this leads further controlled release of Ag ions. Therefore, the presence Ag nanoparticles on the external surface of AC and AC pores to facilitate inactivation of microbes in a more effective manner. As Ag nanoparticles have strong interaction with such functional groups e.g., hydroxyl, carbonyl, carboxyl present on a carssbon basal plane[32,33] a large number of Ag nanoparticles can be embedded strongly on the external surface of AC. Ag-NPs have been reported to be effective in deactivating and inhibiting growth of both Gram negative and Gram positive bacteria, but with more pronounced results shown on the Gram negative bacteria.[34-36] Because of this, combining Ag-NPs with another metal oxide such as zinc oxide nanoparticles (ZnO-NPs), would produce a material with strong antibacterial properties for both Gram negative and Gram positive bacteria[37,38] and hence will expand the antibacterial activities of materials to a wider variety of applications. Moreover, the hybridization of ZnO with Ag immensely increases the rate of electron-transfer process in ZnO, resulting in a better photocatalytic activity compared with that of pure ZnO NPs. Besides, If Ag, ZnO and Ag-ZnO are immobilized on porous hosts, the release time of silver and zinc ions can be delayed, so that such supporting materials will have great potential for use in this application. Hence, in this study we have impregnated individually Ag, ZnO and Ag-ZnO on activated carbon through simple sol-gel route and these nanohybrids evaluated for antimicrobial activity.

2. Results and Discussion

Characterization of the materials

As can be seen from Figure 1, at low relative pressures, a rapid increase in the adsorption–desorption isotherms is observed, which is followed by a plateau at higher relative pressures, indicating a type I isotherm according to the IUPAC classification.[39,40] The type I isotherm represents a material with micro porous structure. As the relative pressure increases ($0.45<p/p_0<0.98$), a broad hysteresis loop was observed, which indicates the presence of meso-porous with a wide pore size distribution (PSD). When the relative pressure was higher than 0.98, an abrupt increase in the amount of adsorbed nitrogen was noted. This might have caused by the presence of macropores. The major uptake occurs at low relative pressures indicating the formation of highly porous materials with narrow pore size distribution.

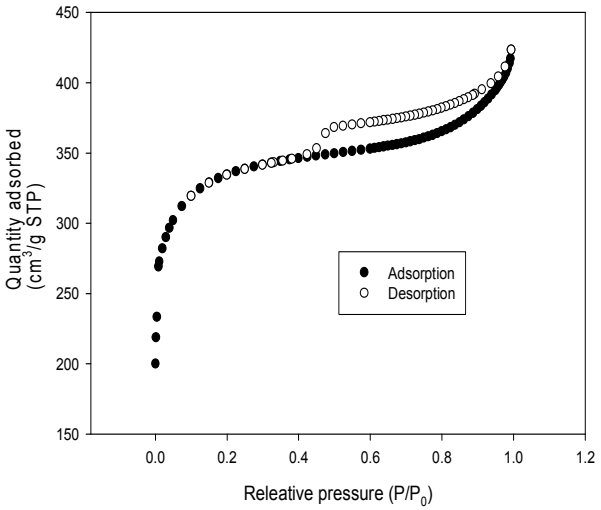

Fig. 1 N_2 adsorption isotherms at −196 °C of AC (p= pressure of the adsorbate and p^0=saturated pressure of adsorptive).

The pore diameter distributions for the AC sample calculated from using DFT (Density Functional theory) model.[41] As can be seen from Figure S1, there is one major peak 5-30 nm shows the presence of mesopores and further it was confirmed from methylene blue (MB) adsoption study from water solution (Figure S2), because the molecular size is 13.82 Å. In order to gain further knowledge of the porous structure of AC, iodine adsorption from liquid phase was adopted. The adsorption of aqueous iodine is considered a simple and quick test for evaluating the surface area of activated carbons associated with pores larger than 1 nm. The iodine adsorption was determined using sodium thiosulphate and it was found to be

1724 m^2/g while N_2 adsorption BET method was found to be 1200 m^2/g. Surface functional groups determined by Boehm titration method,[42] $NaHCO_3$ neutralizes the carboxylic groups, 0.12 mmol/g, Na_2CO_3 neutralizes carboxylic groups and carboxyl groups in lactone, 0.75 mmol/g and the strong alkali (e.g., NaOH) neutralizes all acidic groups including the phenolic hydroxyl groups on a carbon surface, 3 mmol/g. The overall cation ion-exchange capacity of AC was found to be 3.875 mmol/g. To determine the pH_{PZC}, the pH drift method was used.[43] The experimental results are shown in Figure 2. The two curves intersect at 8.5, which is the pH_{ZPC} of the material. Thus it is expected that the surface will have a net positive charge below pH 8.5, and a net negative charge above pH 8.5. When the solution pH was lower than pH_{PZC}, MB dye removal was relatively high, possibly due to the presence of more positive charges on the carbon surface.

The FTIR spectra of pure AC, Ag-AC, ZnO-AC and Ag/ZnO-AC are shown in Figure S3. In the FTIR spectra, bands at 3450 cm^{-1} (m) and 3150 cm^{-1} are due to O-H stretching frequency of water molecule and carboxylic group respectively. A very weak band at 1650 cm^{-1} is for C=C aromatic stretch. Peaks at 1465 and 1383 cm^{-1} are due to C-H bend in CH_3 and peak at 1120 cm^{-1} is for C-O stretch. A new peak at 435 cm^{-1} which may be attributed to the Ag-O bond stretching and peak at 425 cm^{-1} is due to Zn-O bond stretching. This indicates that both Ag and ZnO have been successfully adsorbed on the activated carbon surface. Peak at 673 cm^{-1} can be attributed to the Ag-ZnO nanohybrid formation.[44] The UV-Vis diffuse reflectance spectra of as prepared Ag-AC, ZnO-AC and Ag/ZnO-AC nanostructures are shown in Figure S4. In case of Ag-AC and Ag/ZnO-AC material system show one band centered at about 310 nm. The band at 310 nm attributed to the presence of Ag_5 clusters.[45] ZnO-AC nanohybrid material exhibits one electronic band at 390 nm due to the presence ZnO. All the above DRS spectra reveal that AC does not influence structural alteration of Ag and ZnO structures rather provide a suitable surface for impregnation. However, in all the four systems a common band centered at 215 nm and 250 nm may be due to the amorphous nature of graphitic form.[46]

The powder XRD patterns of all four nanohybrid materials are shown in Figure 3. The pure AC shows two broad diffraction peaks at 2θ angles of 24 and 44 which can be indexed to (002) and (100) diffraction for typical graphite carbons (ICDD 89137). Ag-AC nanohybrid pattern exhibits peaks at 2θ angles of 38.21, 44.41, 64.54, and 77.48 that corresponds to the (111), (200), (220) and (311) crystal planes of a cubic lattice structure of Ag nanoparticles respectively (ICDD 893722). ZnO-AC exhibits peaks at 2θ angles of 31.75, 34.25, 36.32, 47.52, 56.60, 62.85, 66.45, 67.95 and 69.15 hexagonal wurtzite structure of ZnO assigned to the planes (100), (002), (101), (102), (110), (103), (200), (112) and (201) (ICDD 891397). The pattern Ag/ZnO-AC exhibits peaks of Ag, ZnO and AC. It suggests an intra-granular coupling between from all the phases. No other segregations of phases were detected in the XRD. In order to know Ag and ZnO formed separate nanoparticles or embedded into one nanoparticle, the intensity of each peak (Ag and ZnO) in Ag/ZnO-AC showed reduction in intensity. However, the reduction in intensity was more with ZnO compare to Ag. Further, the crystallite size was calculated using Debye-Scherrer formula using most intense peak of Ag (2θ:38.21) and ZnO (2θ:36.32). The analysis revealed that in Ag-AC, ZnO-AC nanohybrid materials size was found to be 42.6 nm, 14.4 nm respectively. While in case of Ag/ZnO-AC nanohybrid material the crystallite size of Ag and ZnO was found to be 52 nm and 22.1nm respectively. An increase in crystallite size of Ag and ZnO phases were due to an intra-granular coupling between from all the phases.[47] Hence, the XRD describes the formation of Ag/ZnO-AC nano nanohybrids. Besides there is AC peak in the XRD pattern of Ag-AC, ZnO-AC and Ag/ZnO-AC mixture, this suggests that crystal structure of Ag and ZnO particles has not modified due to presence of AC.

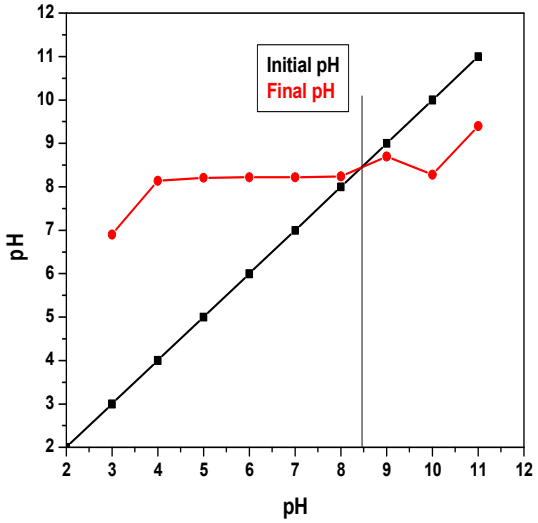

Fig.2 Point of zero charge (pH_{PZC}) of the AC, determined by the pH drift method

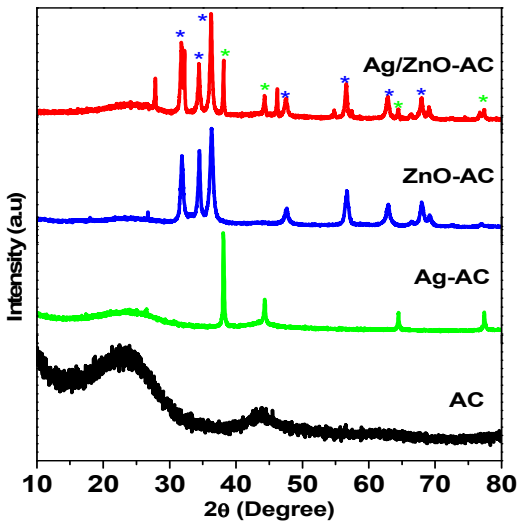

Fig. 3 The XRD pattern of AC, Ag-AC, ZnO-AC and Ag/ZnO-AC nanohybrid material

RSC Advances

ARTICLE

Dynamic light scattering (DLS) is one of the important technique used to determine the particle size of materials. During the DLS measurement, nanohybrid materials dispersed in water phase and the distribution of nanohybrid materials hydrodynamic diameter is shown in the Figure 5S. It revealed that average diameter of Ag-AC, ZnO-AC, Ag/ZnO-AC(Ag) and Ag/ZnO-AC (ZnO) was found to 16.5 nm, 21.1 nm, 18.4 nm and 17.1 nm respectively.

The SEM micrographs of AC particles are shown in Figure 4 exhibits flake shape and display porous character. SE micrographs of **Ag-AC** nanohybrids clearly reveals the uniform distribution of silver nanoparticles over AC surface. Most of the Ag nanoparticles occupied on the surface. The impregnation of Ag nanoparticles partially blocked the porosity of the AC surface, although the nanohybrid still displays porous character. In case of **ZnO-AC** nanohybrids, most of the ZnO nanoparticles occupied on the surface. The impregnation of ZnO nanoparticles partially blocked the porosity of the AC surface, although the nanohybrid still displays porous character. In case of SE micrographs of **Ag/ZnO-AC** nanohybrids, both Ag and ZnO nanparticles impregnated individually.

The composition of the AC, Ag-AC, ZnO-AC and Ag/ZnO-AC nanohybrids are further characterized by EDAX. Almost all the peaks on the curves are ascribed to C, Zn, Ag and O elements and some additional ones. These additional peaks may belong to Cu grid used as sample holder in EDAX instrument. Thus, it is concluded that the prepared samples are composed of C, Zn, Ag and O elements, which is in good agreement with XRD and FTIR. Figure 5(a) shows HR-TEM images of prepared nanonanohybrids samples: In Ag-AC nanohybrids, Ag exhibits spherical shape, whereas in ZnO-AC nanohybrids, ZnO exhibits hexagonal structure. In the case of Ag/ZnO-AC, after loading Ag NPs on ZnO-AC, Ag NPs are well distributed on the surface of ZnO nanostructures can be seen Figure 5. The selected area electron diffraction (SAED) pattern of nanohybrid materials are shown in Figure 5b. It shows clear and organized circular spots which tells about the highly poly crystalline nature of prepared materials. TEM micrographs displayed the size and shape of impregnated on activated carbon shown in Figure 5c. Accordingly, nanohybrid material exhibits rod shapes, spherical and some particles are in irregular shapes. The average diameter of the spherical particle is 5-20 nm, rod shapes average length is 30-40 nm while some of the particle exhibits irregular and agglomerated form size is around 30-45 nm.

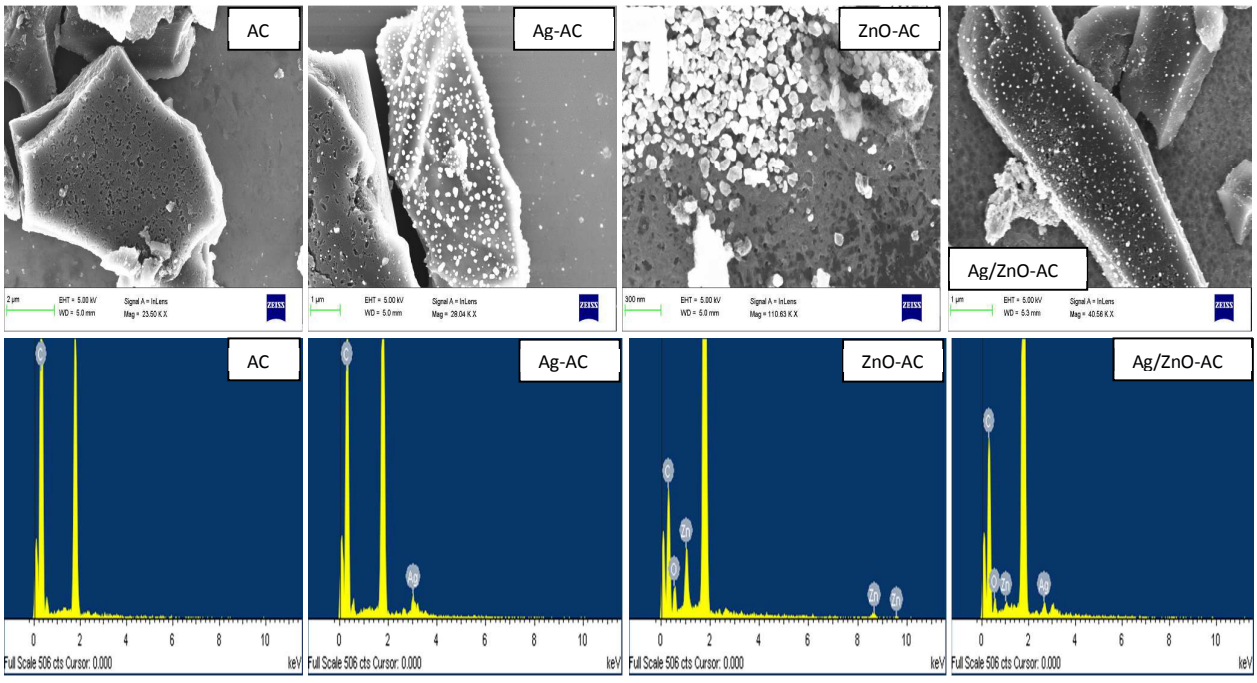

Fig. 4 SEM and EDX images of AC (scale bar: 2μm), Ag-AC (scale bar:1μm), ZnO-AC (scale bar: 300nm) and Ag-ZnO/AC (scale bar: 1μm) nanohybrid materials

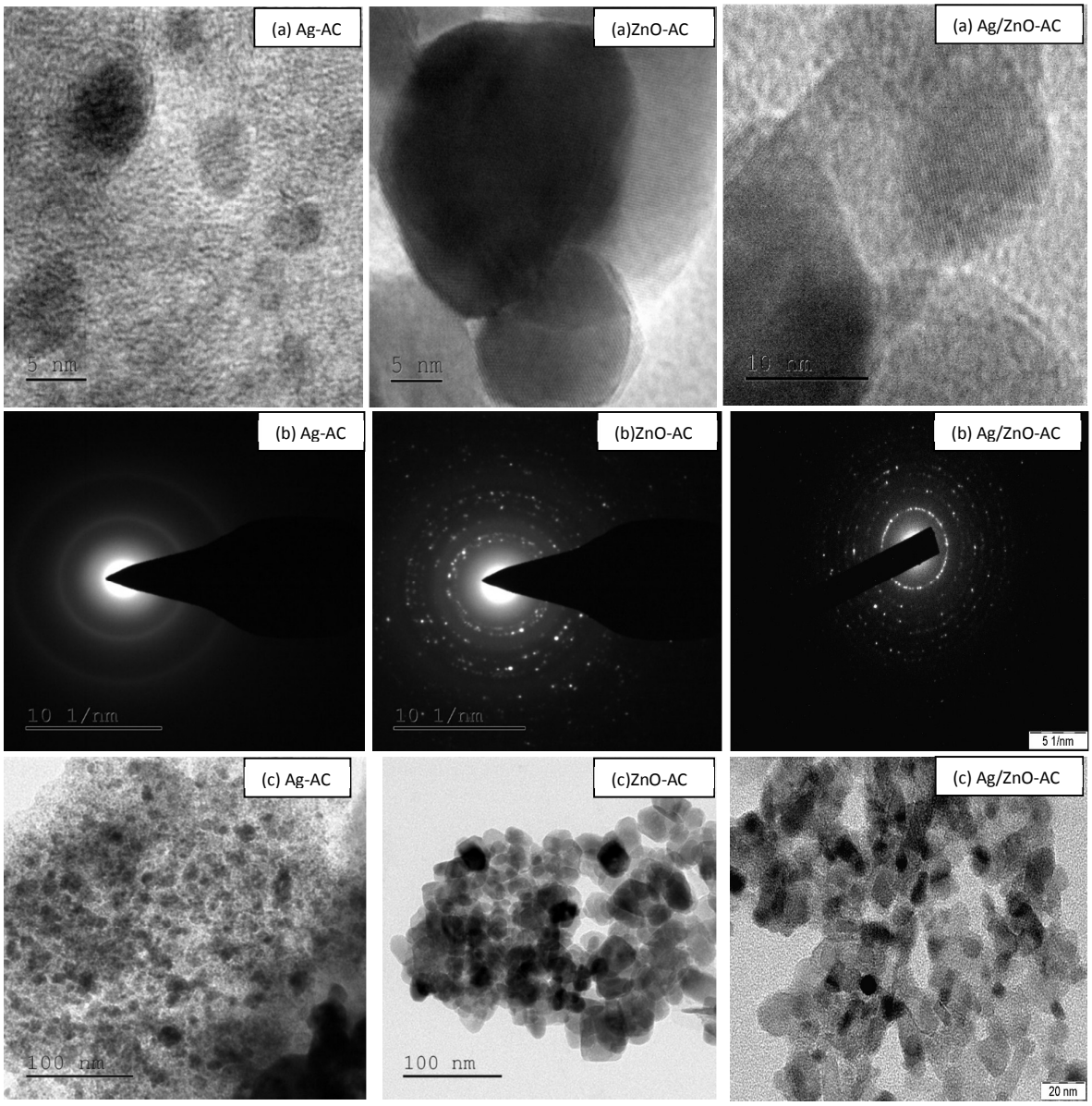

Fig. 5 (a) HRTEM image of Ag-AC, ZnO-AC (scale bar: 5nm), and Ag/ZnO-AC (scale bar 10nm) (b) The SAED pattern of nanocrystalline of Ag-AC, ZnO-AC and Ag/ZnO-AC nanohybrid materials and (c) TEM images of Ag-AC (scale bar: 100nm), ZnO-AC (scale bar:100nm) and Ag/ZnO-AC nanohybrid materials (scale bar:20 nm)

The final application of these nanohybrids used in drinking water treatment and their stability in water was evaluated at different times. Normally when nanoparticles are embedded on certain substrates, water is treated in a fixed bed mode of operation in which the flow conditions are nearly laminar. The vigorous agitation condition adopted for leaching test therefore represented a more adverse condition that may not necessarily be experienced but is important to ensure the material is stable under any circumstance. The accepted concentrations of Ag and ZnO (as Zn^{2+}) in drinking water approved by World Health Organization (WHO) are 0.1 mg/L and 3–5 mg/L, respectively.[48] The AAS measurements showed that the concentrations of silver and zinc were <0.005 to 0.011 mg/l and <0.02 to 0.71 mg/l, respectively. The obtained results indicate therefore that the materials do not pose any danger for drinking water treatment since the leached metals were below the maximum allowable concentrations. Interestingly, the nanohybrid of Ag/ZnO-AC exhibited the minimum leaching of metals (Ag=0.03% and Zn=4.2%) in comparison to the of individual nanohybrids [Ag-AC (Ag=0.56%) or ZnO-AC (Zn=25.8%). The results show that in the case Ag/ZnO-AC there is a strong interaction between metallic Ag and ZnO nanocrystals because of the formation of Zn-O---Ag bonds on the interface (Figure 6). These results indicate that the antibacterial property of Ag/ZnO-AC nanohybrid would be longer.

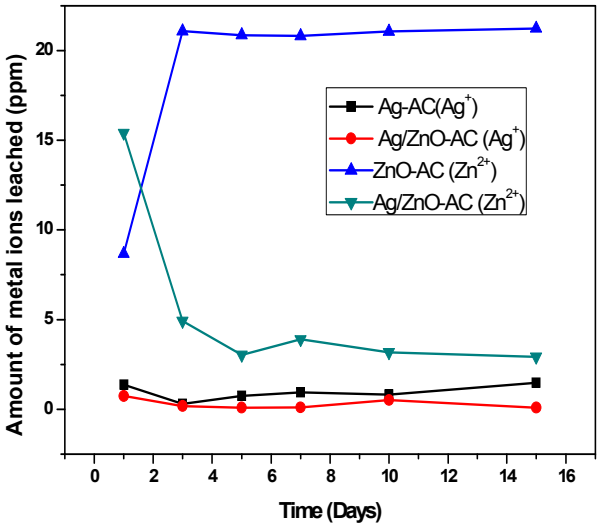

Figure 6: Leaching test performance of AC, Ag-AC, ZnO-AC and Ag/ZnO-AC nanohybrids material in pure water medium

Further, qualitative assessment of antibacterial effect was evaluated by disc diffusion assay and the zone of inhibition (ZOI) and is shown in Table 1 and Figure S6. From the photographs it is clear that the ZOI formed by Ag/ZnO-AC nanohybrid is more compared to other individual nanohybrid materials, suggesting that Ag/ZnO-AC nanohybrid is an efficient antibacterial material for both Gram-negative and Gram-positive bacteria. Because of their size, Ag/ZnO-AC can easily reach the nuclear content of bacteria and they present the large and impressive surface area; thus, the contacts with bacteria were maximum. This could be the reason behind their excellent antibacterial effect and effective antibacterial activity both in Gram negative and Gram positive bacteria's and the results compared with Amikacin standard drug. We did not notice any change in ZOI for the mix of Ag-AC and ZnO-AC compare with individual system. Hence, the order of ZOI was AC< ZnO-AC<Ag-AC<Ag/ZnO-AC.

As shown in Table S1 and Figure S7, the MIC and MBC values of four-against tested pathogens were in the range of 0.20-2.5 mg/ml and 0.35-3.0 mg/ml respectively. While Ag/ZnO-AC nanohybrid material exhibited lowest MIC as well as MBC values compared to other nanohybrid materials. The tests results revealed that a higher MIC and MBC value for *S. aureus* comparing to *E. Coli* pathogens. This may be due to the differences in bacterial cell walls, since Gram negative bacteria have thinner cell wall comparing to Gram positive bacteria. Further, MIC for Ag/ZnO-AC nanohybrid showed much less than that of ZnO-AC and Ag-AC noanohybrid system indicating the synergistic effect of the Ag/ZnO-AC nanohybrid material.

Time Kill Curve analysis: Rate of the bacterial growth killing by these nanohybrids was assessed by time kill curves shown in Figure7 and Figure S8. The test results showed that *E. Coli* microorganism die within 8 h from the time of addition of Ag/ZnO-AC and Ag-AC nanohybrid materials. However, ZnO-AC and AC materials exhibited significant antimicrobial activity against *E.coli*. Decrease in cell count was expressed in $\log_{10}$ CFU ml^{-1} and any reduction <3$\log_{10}$ CFU, relative to the untreated control was considered to be significant.

Table 1: Evaluation of disk diffusion assay values of AC (1), Ag-AC (2), ZnO-AC(3) and Ag/ZnO-AC(4) with amikacin (30µg) (5)]. The standard deviation ranging from ±0.1 to ±0.2 (n=3)

Nano nanohybrid materials	Zone of Inhibition (mm)							
	Gram positive strain				Gram negative strain			
	S. aureus (ATCC-9144)		*B. subtilis* (ATCC-6051)		*P. aerugenosa* (ATCC-2853)		*E. coli* (ATCC-25922)	
	1000 µg	2000 µg	1000 µg	2000 µg	1000 µg	2000 µg	1000 µg	2000 µg
1	8	10	7	9	7	9	7	9
2	9	11	7	10	10	13	6	10
3	8	10	7	11	7	10	8	10
4	10	**14**	8	**11**	8	**16**	6	**14**
5	23		23		22		20	

The post agent effect of AC, Ag-AC, ZnO-AC and Ag/ZnO-AC nanohybrid materials were studied against only on *E. coli* microorganism. The post-exposure effect was sustained 2.45 ± 0.2 h with Ag/ZnO-AC; 2.2 ± 0.1 wih Ag-AC; 2.0 ± 0.2 with ZnO-AC and 0.51 ± 0.15 with AC. The high PAE with Ag/ZnO-AC might be due the photocatalytic material and this effect might be good in reducing the dose and prolonging the time interval of administration thus decreasing any possible adverse effects.

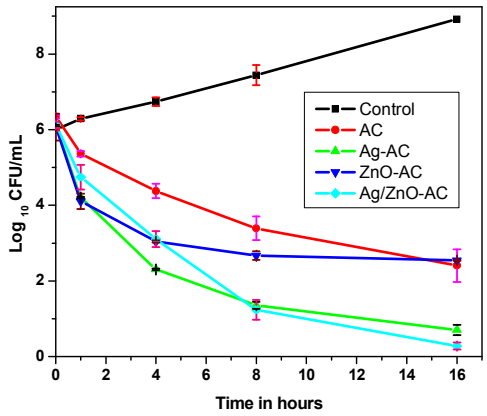

Fig. 7 Kill curve for *E. coil* tested with 4x MIC of individual nanohybrid materials

Possible mechanism

(i) AC used in this work showed an antibacterial activity towards both Gram positive and Gram negative bacteria. This antibacterial activity might be due to various hydrophilic functional groups and hydrophobic graphene layers. Moreover, carbon surface displays groups of acidic and basic character that control its behavior in accordance with the medium. The carbon atoms of the basal plane edges might be combined in variable proportions with different hetero atoms,

generating diverse superficial groups.[49-50] Most of these groups are oxygenated due to the tendency of the carbons to oxidize even at room temperature and hence these functional groups enable to show antibacterial activity to maximum extent. (ii) Silver nanoparticles have the ability to anchor to the bacterial cell wall and subsequently penetrate into it, thereby causing structural changes in the cell membrane like the permeability of the cell membrane and death of the cell. Moreover, there is formation of 'pits' on the cell surface, and there is accumulation of the nanoparticles on the cell surface.[51] It has also been proposed that there can be release of silver ions by the nanoparticles[52] and these ions can interact with the thiol groups of many vital enzymes and inactivate them.[53] Silver is a soft acid, and there is a natural tendency of an acid to react with a base, in this case, a soft acid to react with a soft base.[54] The cells are majorly made up of sulfur and phosphorus which are soft bases. The action of these nanoparticles on the cell can cause the reaction to take place and subsequently lead to cell death. (iii) In case of ZnO-AC, It can be explained based on the oxygen species which released on the surface of ZnO. Generation of highly reactive species such as OH^-, H_2O_2 and O^{2-} generated in the ZnO suspensions and H_2O_2 can cause fatal damage to microorganisms. Since, hydroxyl radical and super oxides are negatively charged particles, they cannot penetrate into the cell membrane and must contact directly the outer surface of the bacteria but H_2O_2 can penetrate into the cell.[55] More recently, Padmavathy *et al.*[56] reported that ZnO is activated by white lights to increase electron-hole pairs.(iv) The antibacterial ability of Ag/ZnO-AC is related to the photocatalysis and metal release process.[57,58] When ZnO nanoparticles are under light irradiation, electron–hole pairs are created. The hole (h^+) reacted with OH^- on the surface of nanoparticles as well as present on AC surface, generating hydroxyl radicals ($OH^•$), superoxide anion (O^{2-}) and perhydroxyl radicals ($HO_2^•$). These highly active free radicals harmed the bacterial cells resulting in decomposition and complete damage.[59] In order to known the interaction behaviour of the all the hybrid materials with the bacterial cells, SEM was done (Figure S9). The above mechanism confirms Ag/ZnO-AC nanohybrid material exhibits synergistic effect on both types of bacteria. A summary of a few selected Ag/ZnO supported on different substrate for different environmental applications are discussed in Table 2S.[59-65] Clearly, there are some similarities exhibited between these materials and Ag/ZnO-AC composite developed in this study.

3. Experimental

Reagents, bacterial strains and growth media

All chemicals used in this study (zinc acetate 98%, silver nitrate 99.8%, and ammonia 25%) were AR grade purchased from Hi Media, Mumbai, India. All reagents were prepared by using deionised water (18MΩ resistivity). Four bacterial cultures were used including two gram positive (*Bacillus subtili* (ATCC-6051), *Staphylococcus aureus* (ATCC-9144) and two gram negative (*Pseudomonas aeruginosa* (ATCC-2853), *Escherichia coli* (ATCC-25922).

Synthesis Scheme

Ag-AC: 1.69 g of silver nitrate was dissolved in 20 ml deionised water. To this solution 1 g commercially available activated carbon (particle size less than 10μm) was added followed by stirring at 40 °C for about 24 h in an Erlenmeyer flask. Later the above suspension was cooled in ice bath for 15 min and sodium borohydride (20 ml, 0.2 N) was added to it slowly with constant stirring for 24 h at room temperature. It was then filtered, washed and dried at 80 °C for 24 h.

ZnO-AC: 2.19 g of zinc acetate was dissolved in 20 ml of deionised water. To this solution 10 ml of 0.5 M hexamethylene tetraamine was added and pH of the solution was maintained 8 using liquid ammonia. To the resulted mixture 1 g AC was added followed by stirring for 24 h at 70 °C in an Erlenmeyer flask. It was then filtered, washed, dried at 90 °C for 24 h.

Ag/ZnO-AC: To the aqueous solution of silver nitrate **(**1.69 g in 20 mL deionised water) 1 g ZnO-AC prepared from the above step was added and stirred solution for (24 h at 40 °C in an Erlenmeyer flask. The obtained suspension was cooled in ice bath for 15 min followed by the addition of sodium borohydride (20 ml, 0.2 N) slowly with constant stirring for 24 h at room temperature. It was later filtered, washed and dried at 80 °C for 24 h.

Characterization of AC, Ag-AC, ZnO-AC and Ag/ZnO-AC nanohybrid materials

Iodine number: It is a widely used technique to determine the adsorption capacity for its simplicity and rapid assessment of activated carbon quality. The iodine number indicates the porosity of activated carbon and it is defined as the amount of iodine adsorbed by 1g of carbon at the mg level. The iodine adsorption was determined using sodium thiosulphate volumetric method.[66]

BET adsorption isotherm: N_2 adsorption–desorption analysis was carried out using Micromeritics ASAP 2020 instrument. The sample used was 0.0275 g. The outgas condition was set to 300 °C under vacuum for 2 h, and all the adsorption–desorption measurements were carried out at liquid nitrogen temperature (-195.542 °C). The original DFT method for the slit pore geometry was used to extract the pore size distribution from the adsorption branch using the Micromeritics software.[67-69] The BJH adsorption cumulative pore volume Harkins and Jura method was used to extract the microporosity.

Acid/Base Titrations (Boehm titration): Surface characteristics (either acidic or basic) of the nanohybrid materials were assessed by the selective acid/base neutralization method developed by Boehm.[70] Aliquots of 0.2 g activated carbon were reacted with 25 mL of 0.1 N NaOH, 0.1 N Na_2CO_3, 0.1 N $NaHCO_3$, and 0.1 N HCl, respectively, for 48 h. Back-titration was carried out using HCl (0.1 N) to neutralize excess base for determining base consumption by the activated carbon. The

consumptions of various bases are related to the properties and amount of functional groups on the carbon surface. Accordingly, $NaHCO_3$ neutralizes the carboxylic groups, Na_2CO_3 neutralizes carboxylic groups and carboxyl groups in lactone, and the strong alkali (e.g., NaOH) neutralizes all acidic groups including the phenolic hydroxyl groups on a carbon surface. The total cation exchange capacity (CEC) was found by the formula:

$$CEC\ (mmol/g) = \frac{(N_1-N_2)\times V}{m}$$

Where N_1 and N_2 are the molarity (mol/L) of the $NaOH/Na_2CO_3/NaHCO_3$ solution before and after equilibrium, respectively; V is the volume (mL) of HCl taken in Erlenmeyer flask, and m is mass (g) of AC used.

Determination of pH_{zpc}: Determination of pH_{zpc} was done to investigate the surface charge of activated carbon.[71] For the determination of pH_{zpc}, 0.01 M NaCl was prepared and its pH was adjusted between 2.0 and 12.0 by using NaOH/HCl. 50 mL of 0.0 1M NaCl was taken in the 250 mL Erylemeyer flask and 0.20 g of activated carbon was added to the solution. After 48h pH of the solution was measured by using a two-point calibration pH meter. Graphs were then plotted between "pH_{final} *versus* $pH_{initial,}$" and the point of interaction of these two curves shows pH_{zpc}.

FTIR analysis: FTIR spectra of the samples were recorded on Nicolet AVATAR 380 FTIR spectrophotometer using potassium bromide (KBr) pellet method. Oven dried solid samples such as activated carbon Ag, ZnO and Ag/ZnO naomaterials impregnated activated carbon were thoroughly mixed with KBr in the ratio 1:100 (weight ratio of sample to KBr). The solid mixture of the sample and KBr were ground to a truly fine powder, and compressed to obtain a thin film disk for the spectrum analysis. The spectra were recorded in the mid-infrared region from 4000 cm^{-1} to 400 $cm^{-1.}$

Diffuse reflectance spectroscopy (DRS): It is used to confirm the presence of Ag and ZnO nanostructures on activated carbon. These studies were carried out by mixing a small amount of metal impregnated activated carbon powder with $BaSO_4$ (as reference material) in 1:100 ratios and the resulting mixture was used for pellet making. The reflectance spectra of the nanohybrid materials over a range of 200–800 nm were recorded with a model JASCO V-570 UV–Visible system with an integrating sphere.

Powder XRD analysis: For determining the phase of the synthesized materials powder X-Ray Diffraction (XRD) patterns were obtained by means of X-ray diffractometer (Bruker D8 AXS GmbH) using Cu target K_α (λ=1.5406 A˚) radiation. The measurements were carried out at room temperature using accelerating voltage 54 kV and applied current 40 mA. It was operated in the step scan rate at 0.05˚ (step time 1s; 2θ: 10-80˚). The 1 mm thick powder sample was placed on a sample holder and the reflection spectra were recorded. Standard ICDD data cards were used for indexing XRD data collected.[72]

Dynamic light scattering (DLS): The particle size distribution of prepared materials were measured by using SZ-100 nanopartica series instruments (Horiba Scientific Ltd., Kyoto, Japan). The measurement carried out at 25°C with a 580 nm laser at a scattering angle of 90°. For the DLS size measurements, nanohybrid materials were suspended in water.

Scanning electron microscopy (SEM): The morphology of AC and its nanohybrid with Ag, ZnO and Ag/ZnO were characterized by Scanning Electron Microscope (SEM) using Carl Zeiss ultra 55 SEM equipped with energy dispersive X-ray analysis accessory (EDAX). The operating voltage was in between 5 and 10 kV. The SEM samples were prepared by drop coating the dispersion on copper grid surface.

Transmission electron microscopic analysis: Morphology and size of the nanohybrid particles were analyzed by High Resolution Transmission Electron Microscope (HRTEM). Elemental mapping and selected area electron diffraction (SAED) were obtained using JEOL 2200F TEM operated at 200 kV. The samples for TEM analyses were prepared by sonicating the nanohybrid materials in isopropanol, followed by drop casting on carbon coated copper grids and subsequent drying.

Atomic absorption spectrophotometer: Quantitative estimation of silver and zinc was determined by atomic adsorption spectrometer (AAS) (VARIAN SPECTRAA 240).

Disc-diffusion assay: The antibacterial activities of all test compounds were carried out by disc diffusion method.[73] The test compounds were taken in dimethyl sulphoxide (DMSO) and used in the concentration of 1000 µg and 2000 µg/disc. The target microorganisms were cultured in Mueller–Hinton Broth (MHB). After 24 h the suspensions were adjusted to standard subculture dilution. The petri dishes containing Muller-Hinton Agar (MHA) medium were cultured with diluted bacterial strain. Disc made of Whatman No.1 filter paper, diameter 6 mm was presterilized and maintained in aseptic chamber. Each concentration was injected to the sterile disc papers. Then the prepared discs were placed on the culture medium. Standard drug Amikacin (30 µg) was used as a positive reference standard to determine the sensitivity of each microbial species tested. Then the inoculated plates were incubated at 37 °C for 24 h. The diameter of the clear zone around the disc was measured and expressed in millimeters as their anti-microbial activity.

MIC and MBC: The lowest concentration (highest dilution) of test reagent preventing appearance of turbidity (growth) is considered to be MIC. MIC was performed according to the standard reference method US National Committee for Clinical Laboratory Standards guidelines [NCCLS 2002]. Extract was dissolved in 10% DMSO. The initial concentration of extract was 2.5 mg/ml and end with 0.035 mg/ml concentration. The initial test concentration was serially diluted two-fold. Each well was inoculated with 5µl of suspension containing 10^8 CFU ml^{-1} of bacteria. The antibacterial agents were incubated for 24 h at 37 °C for bacteria. In order to know how much amount of antibiotics is required to kill bacteria then MBC test is required. It determines the lowest concentration at which an antimicrobial agent will kill a particular microorganism. Further, MBC value was determined by sub culturing the test dilution [which showed no visible turbidity] on to freshly prepared nutrient agar media. The plates were incubated further for 24h at 37 °C. The highest dilution that yielded no

single bacterial colony on the nutrient agar plates was taken as MBC. All experiments were repeated at least three times.

Time kill curve studies: The time kill studies were performed according to NCCLS guidelines.[74] Each isolate was inoculated into three flasks, one as a growth control and one for each molecule. The strain for time kill curve studies were performed in MH broth with an inoculum of 5×10^6 - 1×10^7 CFU/ml in the presence of 4×MIC concentration of molecules individually. A flask of inoculated MH broth with no antibiotic served as a control. The surviving bacteria were counted after 0, 1, 4, 8 and 16 h of incubation at 37 °C by sub culturing 50 µl serial dilutions (in 0.9% NaCl) in to MH plates with a spread plater.

Post Agent Effect (PAE): PAE on one microorganism (*E.coli*) was determined with AC, Ag-AC, ZnO-AC and Ag/ZnO-AC, the viable turbidometric method.[74] This was performed after obtaining the MIC values for both the molecules. Treatment group were prepared with test molecules at concentration 10×MIC and diluted bacterial suspension (final inoculums of 10^6 bacterial/ml) whereas the control group were prepared using MHB and diluted bacterial suspension (final inoculums of 10^6 bacterial/ml). Dilution at 1:1000 was done using MHB after incubating both the treatment and control group for 1 h at 37 °C. 2 µl of the diluted sample was streaked on MHA at 0, 2, 4, 6, 8, 10 and 24 h in order to count the number of colonies present after 24 h of incubation at 37 °C and it was performed in triplicate. Graph $\log_{10}$cfu/ml against time was plotted, where the duration of PAE were obtained from the graphs.

$$PAE = T-C$$

Where, T is the time required for the treated organism to increase $1\log_{10}$cfu/ml following dilution at 1:1000 and C is the time required for the control organism to increase 1 $\log_{10}$ cfu/ml following dilution at 1:1000.

Conclusions

We have prepared three nano hybrid materials such as Ag-AC, ZnO-AC and Ag/ZnO-AC by simple solution impregnation route. The results were very promising since powder XRD analysis and TEM image interpretation confirmed the formation of nanohybrids on the activated carbon surfaces. The MIC of Ag/ZnO-AC nanohybrid was found to be 0.20 mg/ml with *E. coli* and 0.30 mg/ml with *S.aureus* while MBC was found to be 0.35 mg/ml with *E. coli* and 0.6 mg/ml with *S.aureus*. Further, Ag/ZnO-AC nanohybrid material exhibited good killing kinetics which was found to be 3 $\log_{10}$ decreases in 5 h while the post-exposure effect was sustained 2.45 ±0.2 only on *E. coli* microorganism. Among the three nanostructures, Ag/ZnO-AC nanohybrid material showed highest antimicrobial activity on selected microorganisms.

Acknowledgements

The authors would like to thank the Chancellor, VIT University, Vellore, India for providing research facilities. The authors are thankful to Water Initiative Technology, Department of Science and Technology (Government of India) for supporting financial support vide project number No.DST/TM/WTI/2K12/61(G).

References

1 P. Jain and T. Pradeep, Biotechnol. Bioeng., 2005, **90**, 59.
2 N. J. Ashbolt, Toxicology, 2004, **198**, 229.
3 K. A. Reynolds, Water Conditioning and Purification, 2007, **12**, 66.
4 M. L. Cohen, 1992, **257**, 1050.
5 S. Ghosh, P. Chakraborty, P. Saha, S. Acharya, M. Ray, *RSC Adv.,* 2014, **4**, 23251.
6 S. Ghosh, D. Ghosh, P.K. Bag, S.C. Bhattacharya, A. Saha, Nanoscale., 2011, **3**, 1139.
7 M. Fang, J. H. Chen, X. L. Xu, P. H. Yang and H. F. Hildebrand, Int. J. Antimicrob. Agents, 2006, **27**, 513.
8 Q. Li, S. Mahendra, D. Y. Lyon, L. Brunet, M. V. Liga, D. Li, and P. J. J. Alvarez, Water Research, 2008, **42**, 4591.
9 H. Cao, X. Liu, F. Meng and P. K. Chu, Biomaterials, 2011, **32**, 693.
10 M. Lv, S. Su, Y. He, Q. Huang, W. Hu, D. Li, C. Fan and S. T. Lee, Adv. Mater., 2010, **22**, 5463.
11 Y. Zhang, D. T. P. Shareena, H. Deng, H. Yu, *J Environ Sci Health C Environ Carcinog Ecotoxicol Rev*. 2015, **33**, 286.
12 J. S. Kim, E. Kuk, K. N. Yu, J. H. Kim, S. J. Park, H. J. Lee, S. H. Kim, Y. K. Park, Y. H. Park, C. Y. Hwang, Y. K. Kim, Y. S. Lee, D. H. Jeong, M. H. Cho, *Nanomedicine,* 2007, **3**, 95.
13 K. R Raghupathi, R. T. Koodali, A. C. Manna, *Langmuir*, 2011, ***27***, 4020.
14 X. Ding, H. Wang, W. Chen, J. Liu, Y. Zhang, RSC Adv., 2014, **4**, 41993.
15 I. Chauhan, P. Mohanty, RSC Adv., 2014, **4**, 57885.
16 C. P. Adams, K. A. Walker, S. O. Obare and K. M. Docherty, PLoS One, 2014, **9**, e85981.
17 H. Liu, F. Ye, Q. Yao, H. Cao, J. Xie, J. Y. Lee, J. Yang, Scientific Reports, 2014, 4:3969, 1-7.
18 S. M. Dizaj, F. Lotfipour, M. Barzegar-Jalali, M. H. Zarrintan, K. Adibkia, Materials Science and Engineering: C**,** 2014, **44**, 1 278.
19 L. Wei, H. Wang, Z. Wang, M. Yu, S. Chen, RSC Adv., 2015, **5**, 74347.
20 Z. Wei, Z. Zhou, M. Yang, C. Lin, Z. Zhao, D. Huang, Z. Chen, J. Gao, J. Mater. Chem., 2011, **21**, 16344.
21 S. Ghosh, V. S. Goudar, K. G. Padmalekha, S. V. Bhat, S. S. Indi, H. N. Vasan, RSC Advances, 2012, **2**, 930.
22 V. K. Sharma, R. A. Yngard, Y. Lin, *Adv. Colloid Interface Sci.* 2009, ***145***, 83.
23 S. Luo, S. Yang, X. Wang, C. Sun, Chemosphere, 2010, **79**, 672.
24 R. Ma, C. Levard, S. M. Marinakos, Y. Cheng, J. Liu, F. M. Michel, G. E. Brown, and G. V. Lowry, Environ. Sci. Technol., 2012, **46**, 752.
25 V. K. Sharma, R. A. Yngard, and Y. Lin, Adv. Colloid Interface Sci., 2009, **145**, 83.
26 H. Yang, Y. Liu, Q. Shen, L. Chen, W. You, X. Wang and J. Sheng, J. Mater. Chem., 2012, **22**, 24132.
27 V. K. Sharma, J. Environ. Sci. Health. A. Tox. Hazard. Subst. Environ. Eng., 2009, **44**, 1485.
28 M. V. Liga, E. L. Bryant, V. L. Colvin and Q. Li, Water Res., 2011, **45**, 535.
29 A. J. Huh and Y.J. Kwon, J. Control. Release, 2011, **156**, 128.
30 K. Y. Yoon, J. H. Byeon, C. W. Park and J. Hwang, Env. Sci Technol., 2008, **42**, 1251.
31 S. Zhang, R. Fu, D. Wu, W. Xu, Q. Ye, Z. Chen, Carbon, 2004, **42**, 3209.

32 G. Xu, J. Shi, D. Li and H. Zhang, J. Polym. Res., 2009, **16**, 295.
33 J. P. Chen, S. Wu and K. H. Chong, Carbon, 2003, **41**, 1979.
34 A. R. Shahverdi, A. Fakhimi, H. R. Shahverdi and M. S. Minian, Nanomedicine, 2007, **3**, 168.
35 N. R. Srinivasan, P. A. Shankar and R. Bandyopadhyaya, Carbon, 2013, **57**, 1.
36 C. A. D. Santos, A. F. Jozala, A. Pessoa and M. M. Seckler, J. Nanobiotechnology, 2012, **10**, 43.
37 Z. Emami-Karvani and P. Chehrazi, J. Microbiol. Res., 2011, 5, 1368.
38 A. Azam, A. S. Ahmed, M. Oves, M. S. Khan, S. S. Habib and A. Memic, Int. J. Nanomedicine 2012, **7**, 6003.
39 B. Xiao and K. M. Thomas, Langmuir, 2004, **20**, 4566.
40 R. C. Bansal and M. Goyal, Activated Carbon Adsorption, Boca Raton, CRC press, 2005.
41 I. Sondi and B. Salopek-Sondi, J. Colloid Interface Sci., 2004, **275**, 177.
42 Q. L. Feng, J. Wu, G.Q. Chen, F. Z. Cui, T. N. Kim, and J. O. Kim, J. Biomed. Mater. Res., 2000, **52**, 662.
43 Y. Matsumura, K. Yoshikata, S. I. Kunisaki and T. Tsuchido, Appl. Environ. Microbiol., 2003, **69**, 4278.
44 J. R. Morones, J. L. Elechiguerra, A. Camacho, K. Holt, J. B. Kouri, J. T. Ramírez, M. J. Yacaman, Nanotechnology, 2005, **16**, 2346.
45 D. M. Blake, P. C. Maness, Z. Huang, E. J. Wolfrum, J. Huang and W. A. Jacoby, Sep. Pur. Methods, 1999, **28**, 1.
46 N. Padmavathy and R. Vijayaraghavan, J. Biomed. Nanotechnol., 2011, **7**, 813.
47 R. Saravanan, N. Karthikeyan, V. K. Gupta, E. Thirumal, P. Thangadurai, V. Narayanan, A. Stephen, Mater Sci Eng C Mater Biol Appl., 2013, **33**, 2235.
48 I. Matai, A. Sachdev, P. Dubey, S. U. Kumar, B. Bhushan and P. Gopinath, 2014, **115**, 359.
49 B. Xiao and K. M. Thomas, Langmuir, 2004, **20**, 4566.
50 R. C. Bansal and M. Goyal, Activated Carbon Adsorption, Boca Raton, CRC press, 2005.
51 I. Sondi and B. Salopek-Sondi, J. Colloid Interface Sci., 2004, **275**, 177.
52 Q. L. Feng, J. Wu, G.Q. Chen, F. Z. Cui, T. N. Kim, and J. O. Kim, J. Biomed. Mater. Res., 2000, **52**, 662.
53 Y. Matsumura, K. Yoshikata, S. I. Kunisaki and T. Tsuchido, Appl. Environ. Microbiol., 2003, **69**, 4278.
54 J. R. Morones, J. L. Elechiguerra, A. Camacho, K. Holt, J. B. Kouri, J. T. Ramírez, M. J. Yacaman, Nanotechnology, 2005, **16**, 2346.
55 D. M. Blake, P. C. Maness, Z. Huang, E. J. Wolfrum, J. Huang and W. A. Jacoby, Sep. Pur. Methods, 1999, **28**, 1.
56 N. Padmavathy and R. Vijayaraghavan, J. Biomed. Nanotechnol., 2011, **7**, 813.
57 I. Matai, A. Sachdev, P. Dubey, S. U. Kumar, B. Bhushan and P. Gopinath, 2014, **115**, 359.
58 X. Wang, Y. Du and H. Liu, Carbohydr. Polym., 2004, **56**, 21.
59 Y. Qin, C. Zhu, J. Chen, D. Liang and G. Wo, J. Appl. Polym. Sci., 2007, **10**, 527.
60 S. C. Motshekgaa, S. S. Ray, M. S. Onyango and M. N. B. Momba, J. Hazard. Mat., 2013, **262**, 439
61 J. Rashid, M.A. Barakat, N. Salah and S. S. Habib, RSC Adv., 2014, **4**, 56892.
62 D. Yin, Z. Le, B. Liu, M. Wu, *J Nanosci Nanotechnol.* 2012, **12**, 2248.
63 M. Ahmad, E. Ahmed, Z.L. Hong b, N.R. Khalid, W. Ahmed, A. Elhissi, J Alloys and Comp., 2013, **577,** 717.
64. D. H. Yoo, T. V. Cuong, V. H. Luan, N. T. Khoa, E. J. Kim, S. H. Hur, S. H. Hahn, J. Phys. Chem. C, 2012, **116**, 7180.
65. H. R. Pant, B. Pant, H. J. Kim, A. Amarjargal, C. H. Park, L. D. Tijing, E. K. Kim, C. S. Kim, Ceramics International, 2013, **39**, 5083.
66 D4607-94 Standard Test Method for Determination of Iodine Number of Activated Carbon, 2006.
67 J. Olivier, J. Porous Mater., 1995, **2**, 9.
68 J. P. Olivier, Carbon, 1998, **36**, 1469.
69 M. Thommes, K.A. Cychosz and A. V. Neimark, In Novel carbon adsorbents, Elsevier, Oxford, 2012
70 H. P. Boehm, Carbon, 1994, **32**, 759.
71 Y.C. Sharma, A guide to the economic removal of metals from aqueous solutions, John Wiley & Sons, 2012.
72 C. Suryanarayana and M.G. Norton, X-Ray Diffraction: A Practical Approach, Springer Science & Business Media, 1998.
73 National Committee for Clinical Laboratory Standards. Performance Standards for antimicrobial susceptibility testing. 8th Informational Supplement. M100 S12. National Committee for Clinical Laboratory Standards, Villanova, Pa., 2002.
74 W.A. Craig and S. Gudmundsson, The postantibiotic effect. In Antibiotics in laboratory medicine, 4th ed.; Lorian, V. Ed., Williams and Wilkins Co.: Baltimore, MD, 1996.

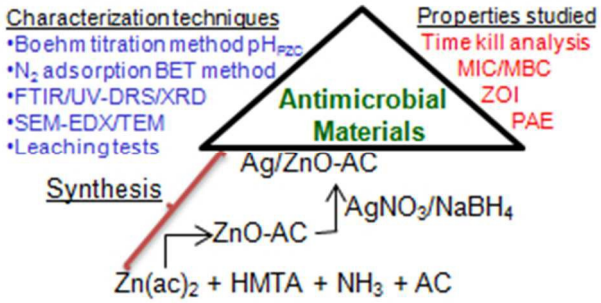

Materials for biological contacts
80x41mm (96 x 96 DPI)